UCRL-10767
c.2

University of California

Ernest O. Lawrence Radiation Laboratory

TWO-WEEK LOAN COPY

This is a Library Circulating Copy which may be borrowed for two weeks. For a personal retention copy, call Tech. Info. Division, Ext. 5545

Berkeley, California

UCRL-10767
c.2

DISCLAIMER

This document was prepared as an account of work sponsored by the United States Government. While this document is believed to contain correct information, neither the United States Government nor any agency thereof, nor the Regents of the University of California, nor any of their employees, makes any warranty, express or implied, or assumes any legal responsibility for the accuracy, completeness, or usefulness of any information, apparatus, product, or process disclosed, or represents that its use would not infringe privately owned rights. Reference herein to any specific commercial product, process, or service by its trade name, trademark, manufacturer, or otherwise, does not necessarily constitute or imply its endorsement, recommendation, or favoring by the United States Government or any agency thereof, or the Regents of the University of California. The views and opinions of authors expressed herein do not necessarily state or reflect those of the United States Government or any agency thereof or the Regents of the University of California.

UCRL-10767

UNIVERSITY OF CALIFORNIA
Lawrence Radiation Laboratory
Berkeley, California

Contract No. W-7405-eng-48

EFFECT OF ANGULAR MOMENTUM ON NEUTRON EMISSION FROM Tb AND Dy COMPOUND NUCLEI

Gabriel N. Simonoff and John M. Alexander

April, 1963

EFFECT OF ANGULAR MOMENTUM ON NEUTRON EMISSION FROM Tb AND Dy COMPOUND NUCLEI

Gabriel N. Simonoff and John M. Alexander

Lawrence Radiation Laboratory
University of California
Berkeley, California

April, 1963

We have studied the production of 4.1-hr Tb^{149g}, 7.4 min Dy^{150} and 17.9 min Dy^{151} by measurements of their α radiations with 2π ionization chambers. These nuclides were produced by two types of reactions involving heavy ions (HI): (a) (HI, xn) Tb^{149g} with x = 3 to 8 (b) (HI, xn)Dy^{149}, Dy^{150} or Dy^{151} with x = 3 to 9. The heavy ions employed were B^{10}, B^{11}, C^{12}, N^{14}, O^{16}, F^{19} and Ne^{20}.

Three kinds of measurements have been made: (a) the range distribution from thin target layers in thin Al catcher foils (b) excitation functions by the stacked foil method (c) angular distribution from thin target layers. The objectives of these experiments were to test the consistency with the compound-nucleus and statistical models and to determine the effects of angular momentum and excitation energy on neutron emission.

I will now show some typical experimental results. First we will consider measurements of the average range R_0. The first figure (from previously reported work)[1] shows the average range of Tb^{149g} produced in a large number of different reactions. These values of R_0 follow a consistent trend when plotted against the recoil energy E_R calculated by assuming compound nucleus formation. In the second figure we present similar results for Dy^{150} and Dy^{151} products. The overall consistency of these data give strong evidence for compound-nucleus formation for all these reactions.

In Fig. 3 we show measured cross section σ divided by calculated total reaction cross section σ_R,[2] for many reactions of type (HI, xn)Tb^{149g}. Note that the peak cross sections are rather low and that they decrease with increasing x. Average angular momentum of the compound nuclei increases with x. It is interesting to compare an excitation function for (HI, xn)Tb^{149g} with that for a typical (HI, xn)Dy^{150} reaction. This comparison, given in Fig. 4, shows that the latter reaction has a much larger cross section and peaks at a much higher energy. This is a general feature of the reactions (HI, xn)Dy^{149}, Dy^{150} or Dy^{151} as indicated in Fig. 5. The striking differences shown in Fig. 4 are attributed to the unobserved 4.0 min Tb^{149m} of higher spin.[3]

We can compare the decay of a compound nucleus, such as Dy^{156}, formed with different projectiles and therefore different average angular momenta. A comparison of the reactions C^{12} + Nd^{144} and Ne^{20} + Ba^{136} is shown in Fig. 6. The latter reactions lead to broader excitation functions and displacement toward higher excitation energies.

We have measured angular distributions for several of these reactions at various energies. The effect of target thickness on a measured angular distribution is shown in Fig. 7. For the average value of the laboratory angles $\langle\theta_L\rangle$ and $\langle\theta_L^2\rangle^{1/2}$ it is possible to correct for target thickness by extrapolating to zero target thickness as shown in Fig. 8. Thus we can characterize each angular distribution by the average squared angle $\langle\theta_L^2\rangle$.

These various measurements can be used to obtain information about (a) the effects of angular momentum (b) the average total energies of neutrons and photons (c) the nuclear temperature as a function of excitation energy and (d) the average angular momenta removed by neutrons and photons.

As previously stated the average range data give evidence that these neutron emitting reactions proceed through a compound nucleus mechanism.[1]

From comparisons of the excitation functions for (HI, xn)Tb^{149g} reactions with those for (HI, xn)Dy reactions, we can infer that only compound systems of angular momentum less than 7.5 $\hbar$ contribute to the former reactions.[4] The compound nuclei of higher spin decay preferentially to 4.0 min Tb^{149m}.

If the neutron emission is isotropic the average squared angle $\langle\theta_L^2\rangle$ can be related to the average total kinetic energy, (T_n) of the emitted neutrons.[5] The average total photon energy T_γ can then be obtained from the total available energy $E_{c.m.} + Q$, $T_\gamma = E_{c.m.} + Q - T_n$.

For reactions of $x = 3$ to 7 we show in Fig. 9 the values of T_γ (deduced from $\langle\theta_L^2\rangle$) as a function of available energy. There is a striking difference between the reactions (HI, xn)Tb^{149g} involving compound nuclei of low spin and the "normal reactions" (HI, xn)Dy^{149}, Dy^{150}, or Dy^{151}. For the latter reactions T_γ increases rapidly with available energy from almost 0 to about 30 MeV. Another way of presenting the results is in terms of the average kinetic energy T_n/x of the neutrons as shown in Fig. 10. For the "normal reactions" average neutron energy increases slowly with available energy. We recall from Fig. 5 that the "normal reactions" peak at ~ 5.5 to 6 MeV per neutron. Thus in Fig. 10 by comparison of the different reactions at a value of $(E_{c.m.} + Q)/x$ of ~ 6 MeV per neutron, an increase of average neutron energy with x is apparent. This reflects a nuclear temperature that increases with excitation energy.

The excitation functions can be used to obtain a quantity $\langle E \rangle_x$, defined as follows

$$\langle E \rangle_x = \frac{\int_0^\infty EF_x(E)\, dE}{\int_0^\infty F_x(E)\, dE} .$$

The fraction of the reactions in which only neutrons are emitted in denoted by F_x. We show the differences between $\langle E \rangle_x$ and the sum of the neutron binding energies in Fig. 11. An increase with average angular momentum can be seen. By comparing the displacements of the lines in Fig. 11 with the values of T_n/x, an idication is given that the average angular momentum removed by each neutron is ~ 3 ħ.[6] An overall angular momentum and energy balance leads to 1.8 ± 0.6 ħ for the average angular momentum removed by each photon.[6,7]

FOOTNOTES AND REFERENCES

*This work was done under the auspices of the U. S. Atomic Energy Commission.

1. L. Wineberg and J. M. Alexander, Phys. Rev. 121, 518 and 529 (1961); J. M. Alexander and D. H. Siscon, Phys. Rev. 128, 2288 (1962).

2. T. D. Thomas, Phys. Rev. 116, 703 (1959).

3. R. D. Macfarlane, Phys. Rev. 126, 274 (1962).

4. J. M. Alexander and G. N. Simonoff, UCRL-10525, October 1962.

5. G. N. Simonoff and J. M. Alexander, UCRL-10099-Rev., September 1962.

6. J. M. Alexander and G. N. Simonoff, UCRL-10541, January 1963.

7. J. M. Mollenauer, Phys. Rev. 127, 867 (1962).

FIGURE CAPTIONS

MU-22787 Fig. 1. Average range as a function of calculated recoil energy for reactions leading to 4.1-hr Tb^{149}. The symbols are as follows: C^{12}, □; N^{14}, ◇; N^{15}, D; O^{16}, Δ; O^{18}, ▽; F^{19}, ⬡; Ne^{20}, ⬡; Ne^{22}, ○. Four bars are for reactions forming compound nuclei for Z = 69; three bars for Z = 68; two bars for Z = 67; one bar for Z = 66; no bars for Z = 65.

MU-26039 Fig. 2. Average range R_0 in Al vs the calculated recoil energy E_R. Symbols are as follows: Dy^{151} ⊡; Dy^{150} △; Dy^{149} ⊙; Open symbols are for the reactions $C^{12}+Nd^{144}$; closed, for $O^{16}+Ce^{140}$. The smooth curve is from reference 1.

MUB-1409 Fig. 3. Cross section σ divided by calculated total reaction cross section σ_R (reference 2) for $(HI,xn)Tb^{149g}$ reactions. The various projectiles, targets, and reactions are indicated. Excitation energies were calculated from Seeger's mass formula; P.A. Seeger, Nucl. Phys. 25, 1 (1961).

MU-28507 Fig. 4. Cross section σ divided by total reaction cross section σ_R (reference 2) versus available energy per emitted neutron $(E_{c.m.} + Q)/x$ for two (HI,xn) reactions.

MU-26040 Fig. 5. Fraction of the calculated reaction cross section vs available energy per emitted neutron. The symbols are as in Fig. 2. Total reaction cross sections are from reference 2.

MUB-1575 Fig. 6. Measured cross section σ divided by calculated total reaction cross section σ_R as a function of excitation energy E.

MU-26037 Fig. 7. The effect of target thickness on observed angular-distribution. The target thickness W is denoted for each curve in $\mu g/cm^2$. These data are for the reaction Nd^{144} + 123-MeV $C^{12} \rightarrow Dy^{149}$ + 7n.

MU-26038 Fig. 8. The dependence of (a) the average angle $\langle \theta_L \rangle$ and (b) the root-mean-square angle $\langle \theta_L^2 \rangle^{1/2}$ on target thickness W. Curves A are for the reaction Nd^{146} + 104-MeV $B^{11} \rightarrow Tb^{149g}$ + 8n;
B for Nd^{144} + 123-MeV $C^{12} \rightarrow Dy^{149}$ + 7n;
C for Ce^{140} + 139-MeV $O^{16} \rightarrow Dy^{149}$ + 7n; and
D for Ce^{140} + 111-MeV $O^{16} \rightarrow Dy^{149}$ + 7n.
The numbers in parentheses denote the slopes of the curves in $deg/(\mu g/cm^2)$.

MU-28462 Fig. 9. Total photon energy vs total available energy. The upper curves are for Tb compound nuclei and the product Tb^{149g}. The lower curves are for Dy compound nuclei and products Dy^{149}, Dy^{150} and Dy^{151}. The number of emitted neutrons is indicated for each curve. Symbols are as follows:

$Pr^{141}(C^{12}, 4n)Tb^{149g}$ ◇; $Nd^{146}(B^{10}, 7n)Tb^{149g}$ θ ;
$Nd^{146}(B^{11}, 8n)Tb^{149g}$ ▽; $Nd^{142}(C^{12}, 3n)Dy^{151}$ X ;
$Nd^{142}(C^{12}, 4n)Dy^{150}$ ⊗; $Nd^{142}(C^{12}, 5n)Dy^{149}$ ⊠;
$Nd^{144}(C^{12}, 5n)Dy^{151}$ □; $Nd^{144}(C^{12}, 6n)Dy^{150}$ △;
$Nd^{144}(C^{12}, 7n)Dy^{149}$ ○; $Ce^{140}(O^{16}, 5n)Dy^{151}$ ▣;
$Ce^{140}(O^{16}, 6n)Dy^{150}$ ▲; $Ce^{140}(O^{16}, 7n)Dy^{149}$ ▲.

MUB-1408 Fig. 10. Average total energy of photons (a) and average energy of neutrons (b) vs available energy per emitted neutron $(E_{c.m.} + Q)/x$ for reactions in which x neutrons are emitted. Symbols are as in Fig. 9.

MU-29076 Fig. 11. The average excitation energy $\langle E \rangle_x$ minus the sum of the binding energies B_i of the neutrons as a function of the average angular momentum $\langle J \rangle$. Different symbols are used for the different (HI,xn) reactions ◈, x = 3; ▽, x = 4; ◎, x = 5; , x = 5; ▣, x = 6; ▲, x = 7; ◍, x = 8; ▟, x = 9. Open points are for Dy^{149}; closed for Dy^{150}; and half open for Dy^{151}.

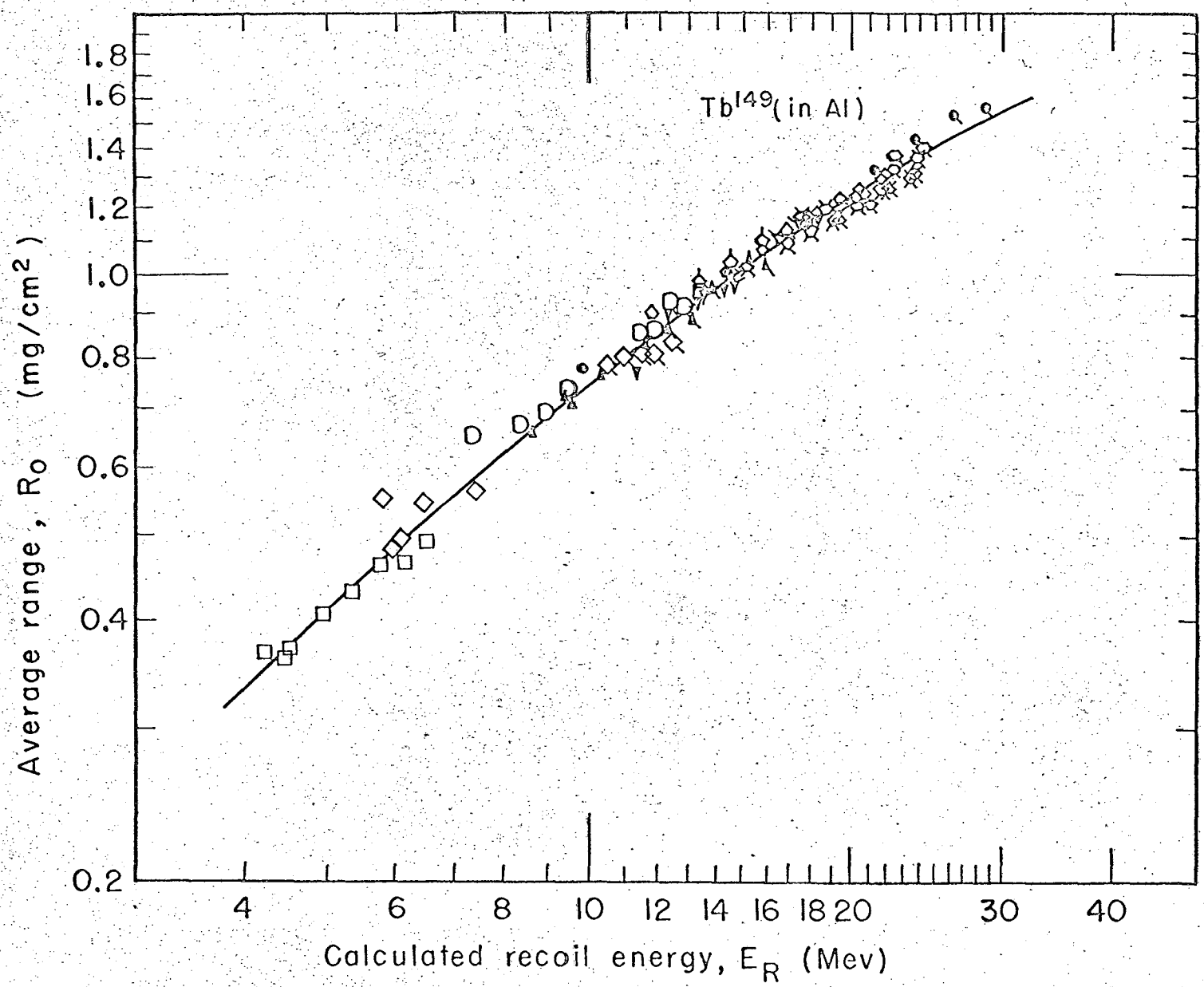

Fig. 1

MU-22787

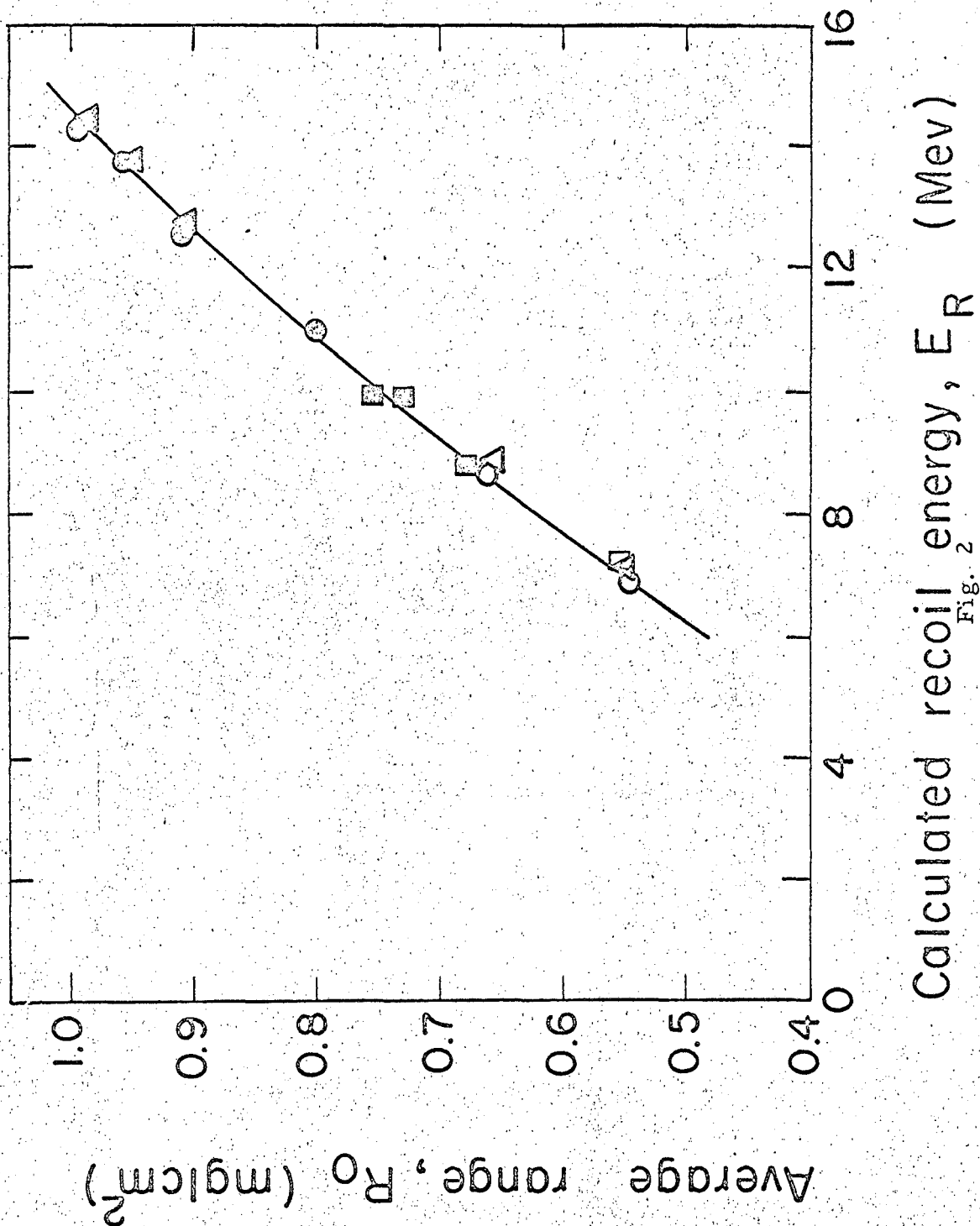

Fig. 2

MU-26039

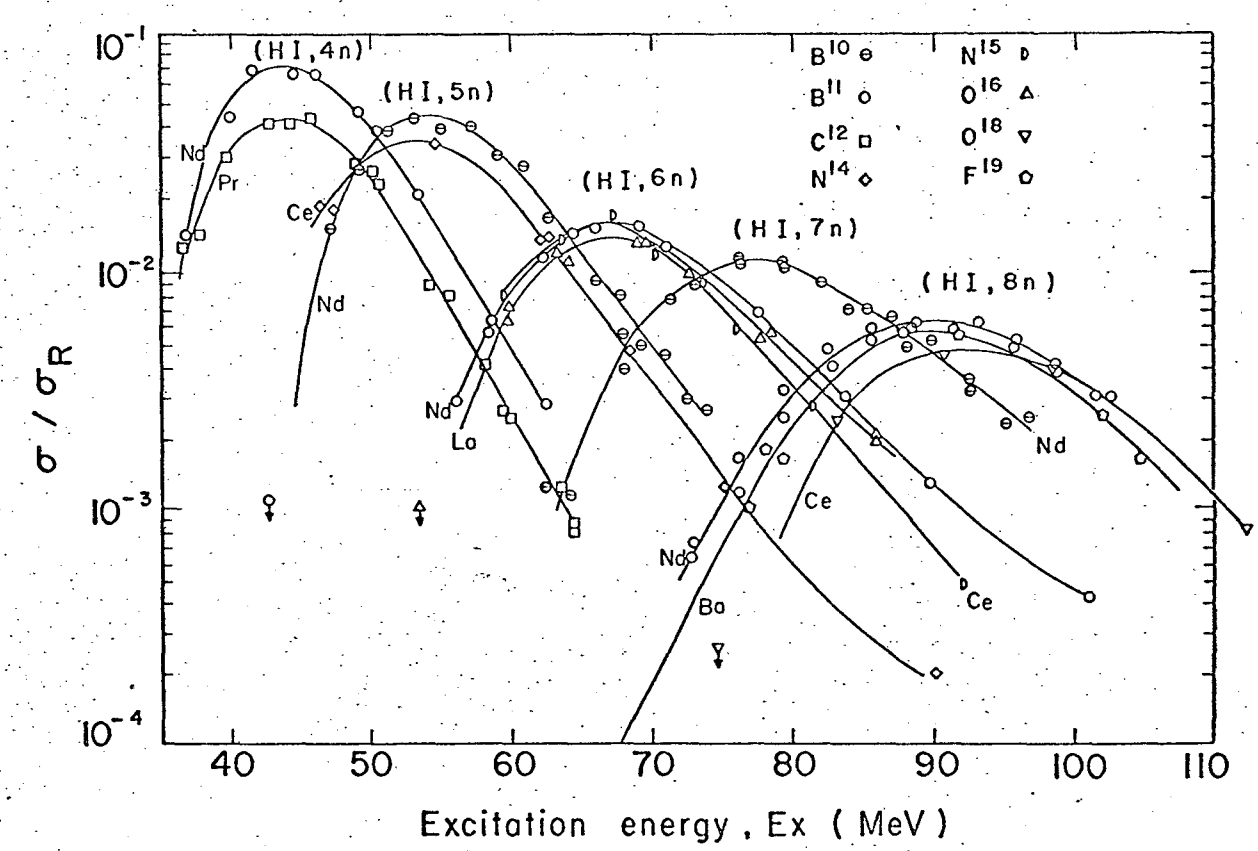

Fig. 3

MUB-1409

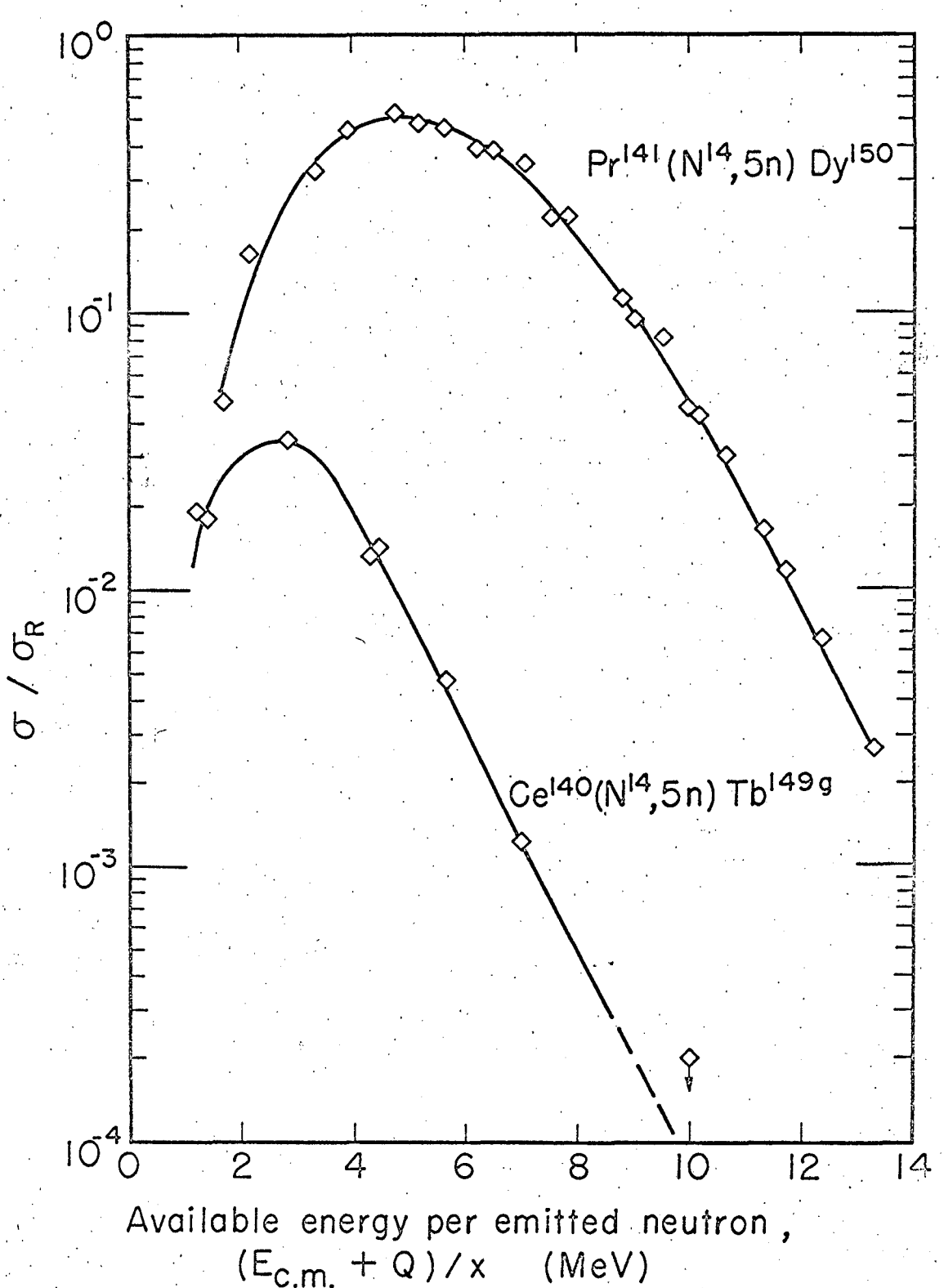

Fig. 4

MU-28507

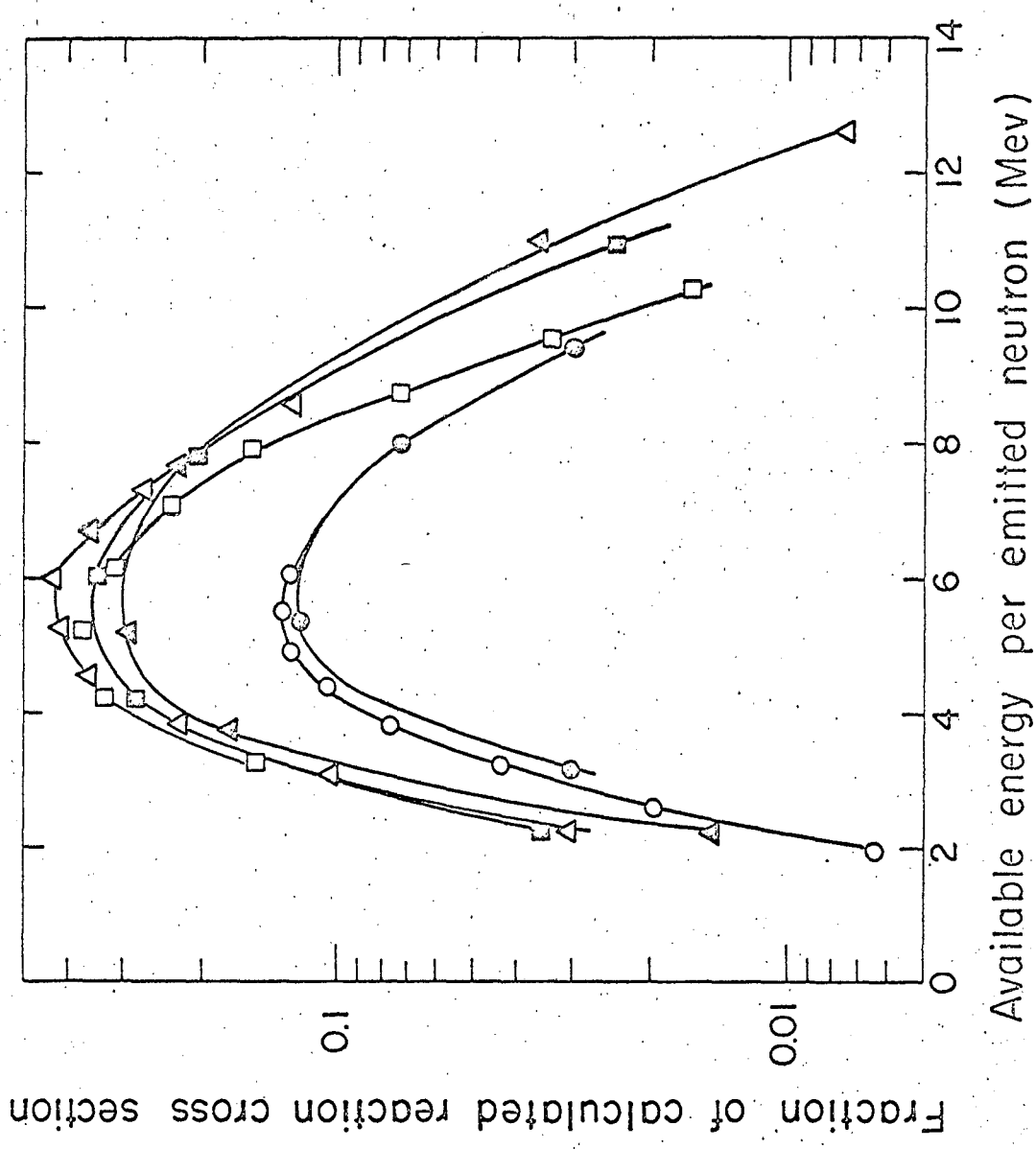

MU-26040

Fig. 5

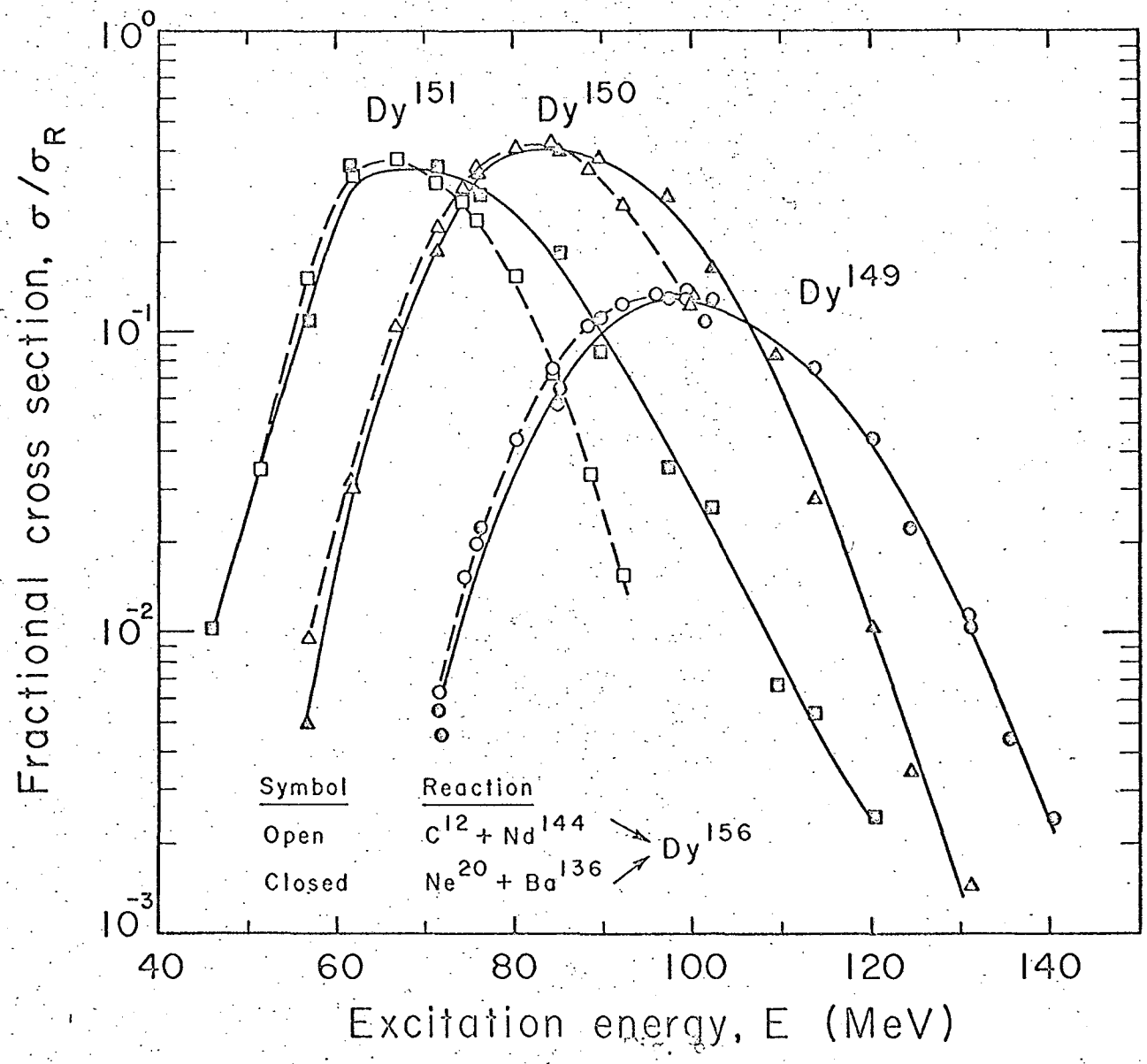

Fig. 6

MUB-1575

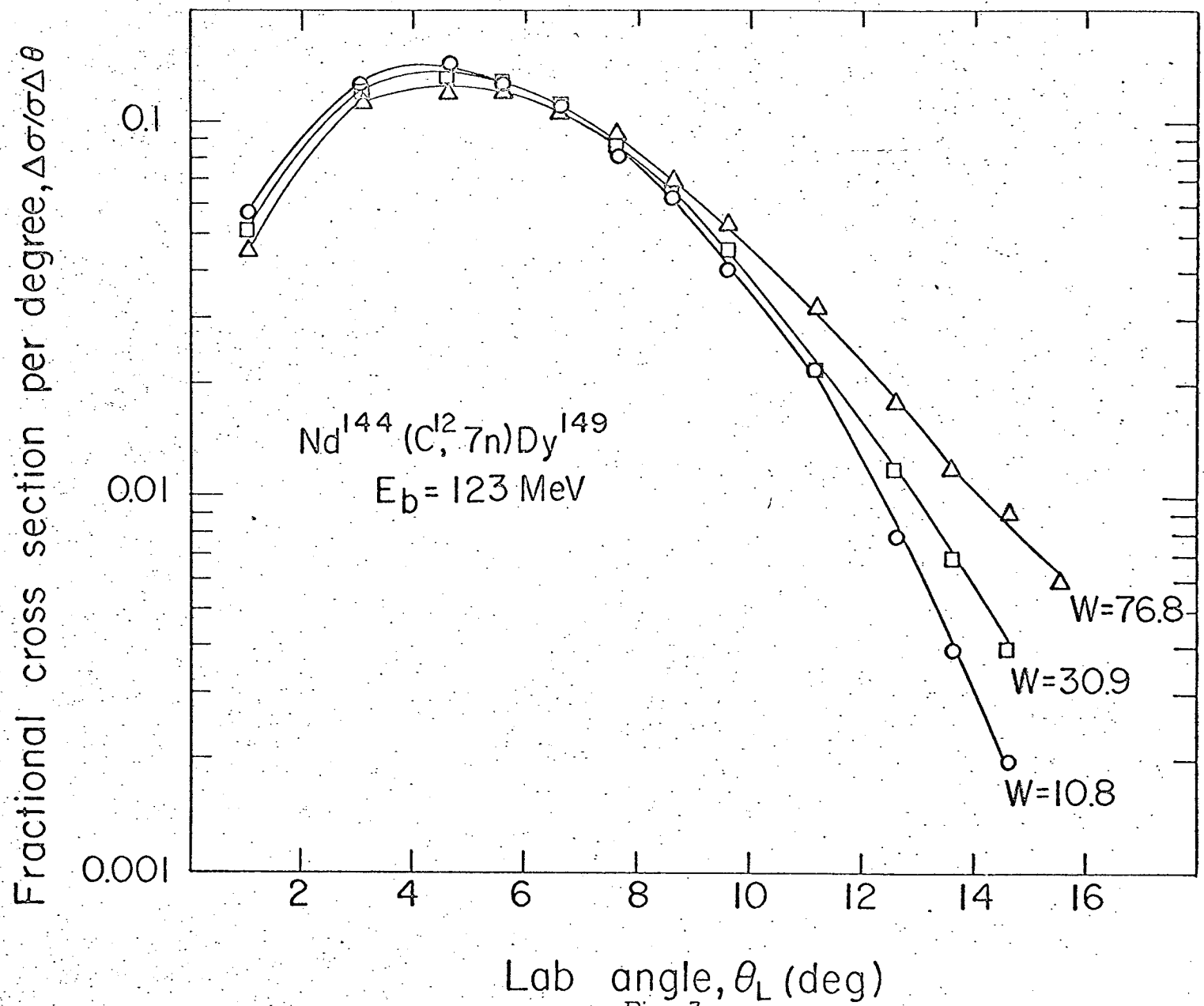

Fig. 7

MU-26037

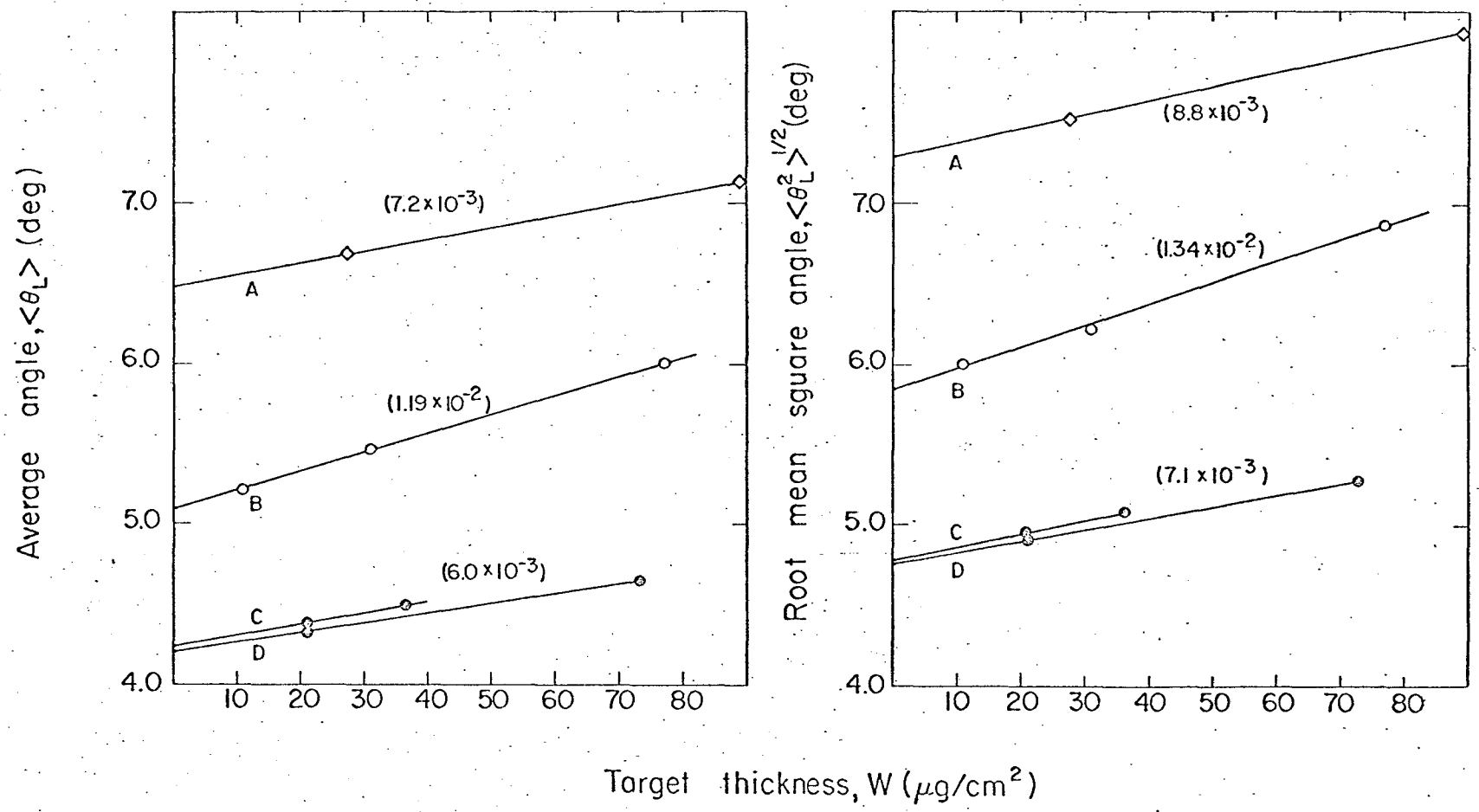
Average angle, $\langle\theta_L\rangle$ (deg)
7.0
6.0
5.0
4.0
(7.2 x 10^{-3})
A
(1.19 x 10^{-2})
B
(6.0 x 10^{-3})
C
D
10 20 30 40 50 60 70 80
Root mean square angle, $\langle\theta_L^2\rangle^{1/2}$ (deg)
(8.8 x 10^{-3})
A
(1.34 x 10^{-2})
B
(7.1 x 10^{-3})
C
D
Target thickness, W (μg/cm^2)
MU-26038

Fig. 8

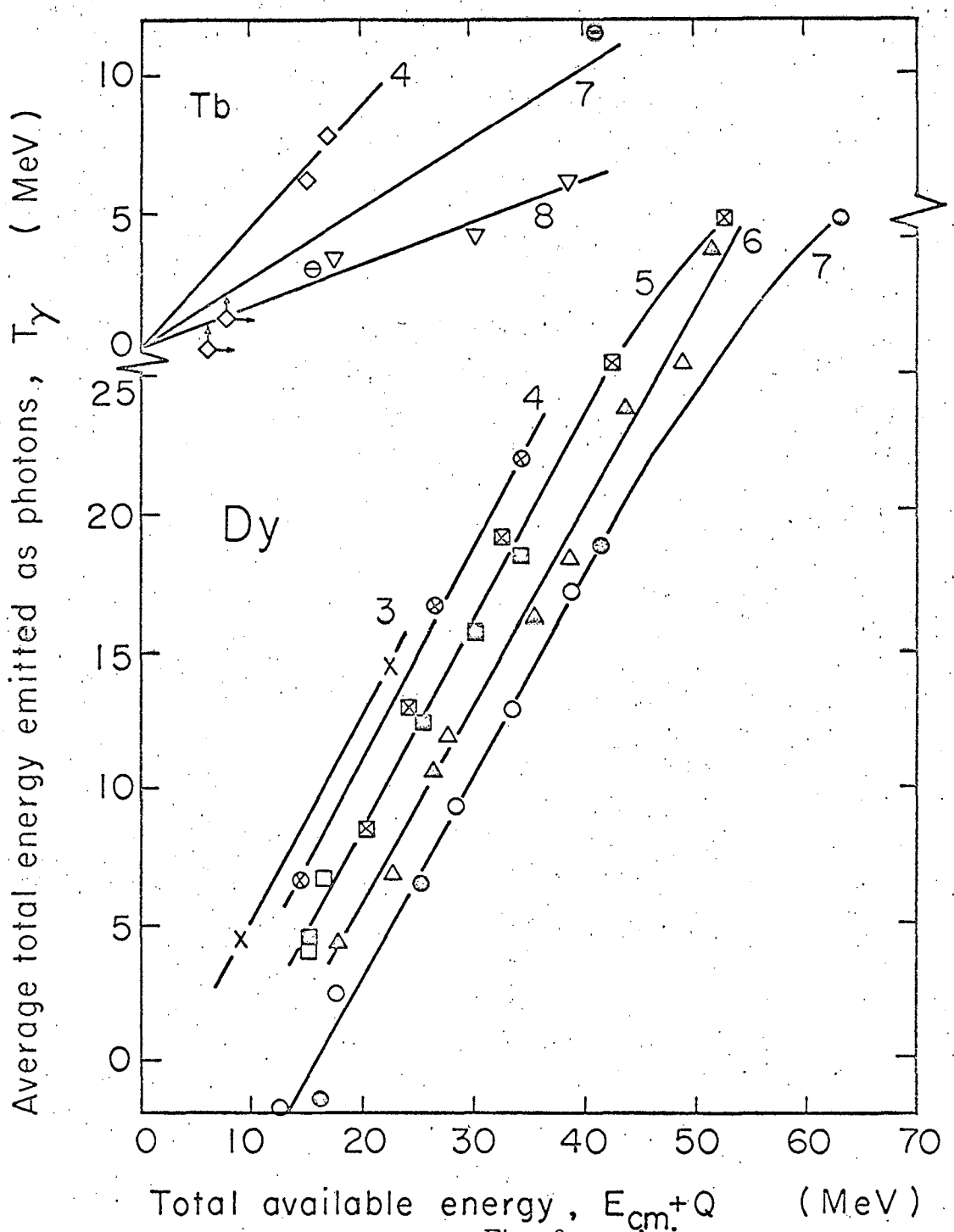

Fig. 9

MU-28462

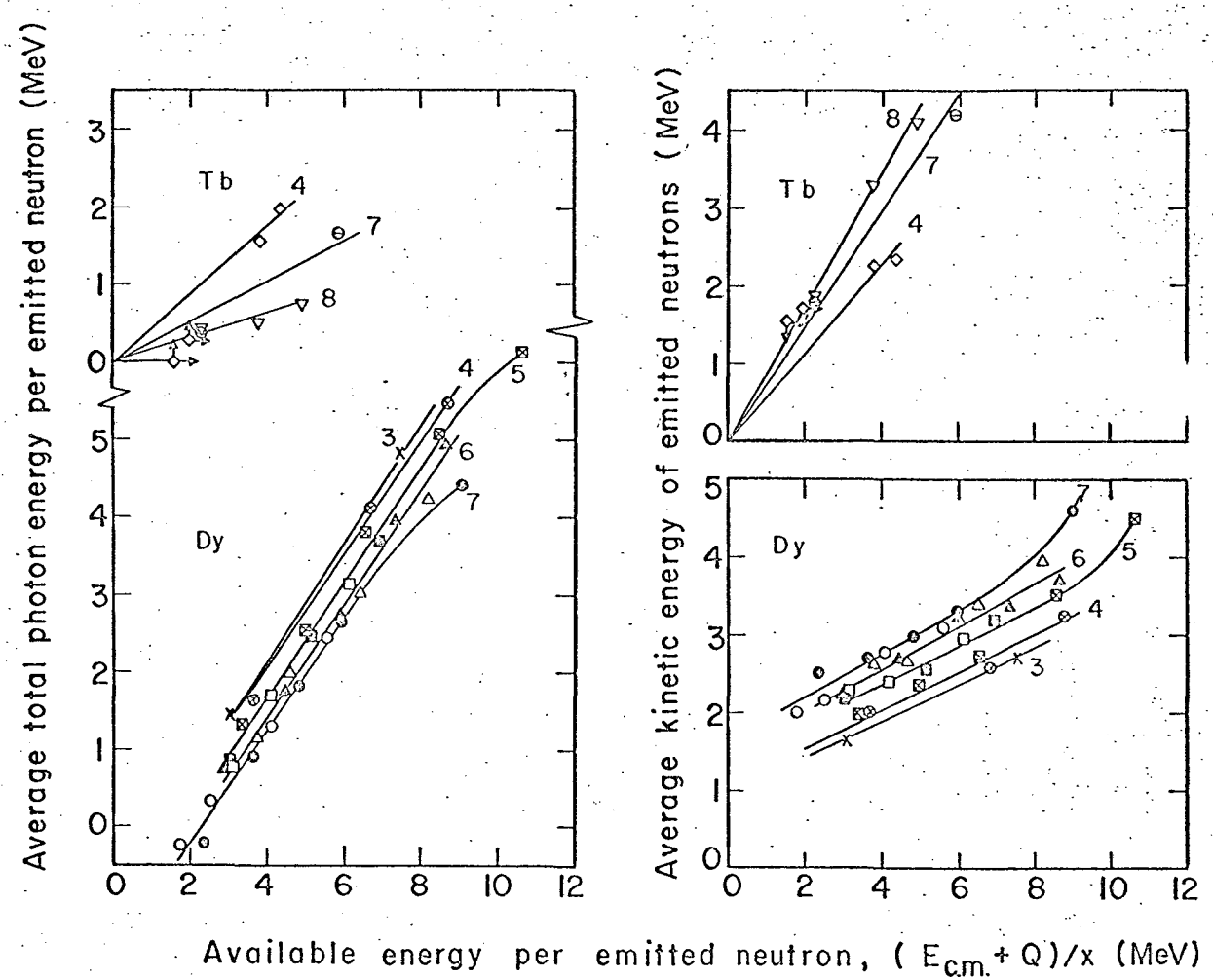

Fig. 10

MUB-1408

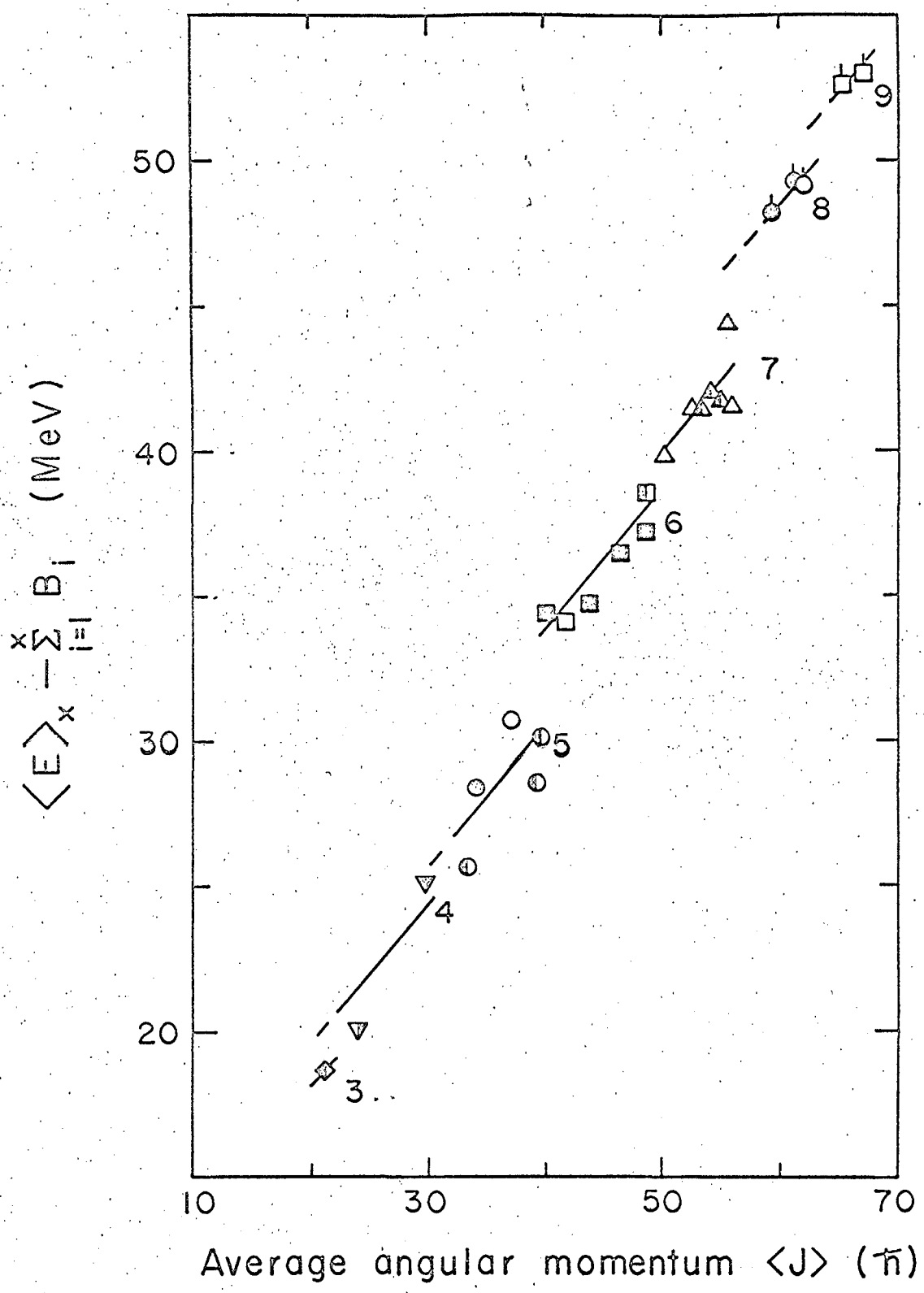

Fig. 11

MU-29076